Journal of Thermal Analysis and Calorimetry (2019) 136:1333–1345
https://doi.org/10.1007/s10973-018-7826-2

Thermal performance improvement in water nanofluid/GNP–SDBS in novel design of double-layer microchannel heat sink with sinusoidal cavities and rectangular ribs

Erfan Khodabandeh[1] · Seyed Alireza Rozati[2] · Mohammad Joshaghani[3] · Omid Ali Akbari[4] · Soheil Akbari[5] · Davood Toghraie[6]

Received: 30 July 2018 / Accepted: 7 October 2018 / Published online: 13 October 2018

Abstract

In this numerical study, laminar flow of water nanofluid/GNP–SDBS (graphene nanoplatelet–sodium dodecylbenzene sulfonate) for 0–0.1% solid nanoparticles mass fraction was investigated for Reynolds numbers of 50–1000 in 3D space via finite volume method. In the newly proposed microchannel design, the cooling fluid is moving in countercurrent in the upper and lower layers of the microchannels, and there are cavities and sinusoidal routes on the solid walls of the microchannel, and the presence of rectangular ribs on the flow centerline along the fluid path enhances mixing for cooling fluid and creates better heat transfer for warm surfaces. The results of this study show that this special design of the microchannel can have a substantial increase in Nusselt number and heat transfer so that in the considered geometry by adding solid nanoparticles mass fraction it is possible to increase average Nusselt number for each Reynolds number by approximately 20%. Also, the mixing of the fluid because of formation of secondary flows has a strong effect on making the temperature distribution uniform in the cooling fluid and solid bed (wall) of the microchannel, especially in the lower layer. The upper layer of the microchannel always has a lower temperature due to indirect contact with heat flux compared with the lower layer. In this study, by increasing Reynolds number and mass fraction of solid nanoparticles the Nusselt number is increased and heat resistance of the lower wall of the microchannel is reduced. Based on the investigation of flow field and heat transfer, the use of the proposed design of the microchannel is recommended for Reynolds number less than 300.

Keywords Novel microchannel design · Sinusoidal cavities · Rectangular rips · Water nanofluid/GNP–SDBS · Nusselt number · Double-layer microchannel heat sink

Nomenclature

C	Mass fraction/wt%
C_p	Specific heat capacity/J Kg^{-1} K^{-1}
g	Gravitational acceleration/ms^{-2}
H	Height/m
k	Thermal conductivity coefficient/$Wm^{-1}k^{-1}$
P	Pressure/Pa
Re	Reynolds number
U	Velocity/ms^{-1}—x direction
v	Velocity/ms^{-1}—y direction
w	Velocity/ms^{-1}—z direction

✉ Davood Toghraie
Toghraee@iaukhsh.ac.ir; davoodtoghraie@gmail.com

[1] Mechanical Engineering Dept, Amirkabir University of Technology (Tehran Polytechnic), 424 Hafez Avenue, P.O. Box 15875-4413, Tehran, Iran

[2] Mechanical Engineering Dept, Isfahan University of Technology, Isfahan, Iran

[3] Civil Engineering Dept, University of Louisville, Louisville, USA

[4] Young Researchers and Elite Club, Khomeinishahr Branch, Islamic Azad University, Khomeinishahr, Iran

[5] Department of Chemical Engineering, Iran University of Science and Technology (IUST), Iran Narmak, Tehran 16846-13114, Iran

[6] Department of Mechanical Engineering, Khomeinishahr Branch, Islamic Azad University, Khomeinishahr, Iran

Greek symbols

μ Viscosity/Pa s
ρ Density/kgm^{-3}

Subscripts

f Fluid
In Inner
Out Outer
p Particle

Introduction

Microchannel heat sinks are one of the most efficient solutions to heating and cooling the equipment. Nanofluids, which are fluids containing suspensions of nanoparticles, have been reported to possess substantially higher thermal conductivity than anticipated from the effective medium theories. Recently, nanotechnology gains interest to explore the microchannel cooling benefits of nanofluids as working fluid [1–9]. Lin et al. [10] optimized the geometry and flow rate distribution for double-layer microchannel heat sink. The optimal design variables were obtained at fixed pumping powers, coolant volumetric flow rates and pressure drops through the MCHS, respectively. Sakanova et al. [11] optimized and compared double-layer and double-layer microchannel heat sinks with nanofluid for power electronics cooling. Their results indicated the nanofluids at a higher concentration yield a better cooling performance by about 17.3% at 5% concentration and 10.6% at 1% concentration. Mohebbi et al. [12] studied convection heat transfer of Al2O3–water nanofluid turbulent flow through internally ribbed tubes with different rib shapes. They observed that the ribbed tubes with Al_2O_3–water nanofluid flow are thermodynamically advantageous. Akbari et al. [13] studied the impact of ribs on flow parameters and laminar heat transfer of water–aluminum oxide nanofluid with different nanoparticle volume fractions in a three-dimensional rectangular microchannel. They observed that an increase in nanoparticle volume fractions causes nanofluid heat transfer properties to have a higher heat transfer and friction factor compared with the base fluid used in cooling due to an increase in viscosity. Leng et al. [14] presented an improved design of double-layer microchannel heat sink with truncated top channels. They concluded that the simulations confirm the effectiveness of the improved design which reduces not only the overall thermal resistance of the heat sink but also the maximum temperature difference on the bottom wall as compared to the original design. Wang et al. [15] investigated geometric parameters on flow and heat transfer performance of microchannel heat sinks. They found that the increase in channel number reduces the thermal resistance, but at the expense of high-pressure drop. Osanloo et al. [16] studied performance enhancement of the double-layer microchannel heat sink by the use of tapered channels. They concluded that thermal performance was improved through increasing the channels convergence angle, although more pressure drop occurred and therefore increased pumping power was required. Arabpour et al. [17] investigated the effects of slip boundary condition on nanofluid flow in a double-layer microchannel. Their results showed that by enhancing the volume fraction of nanoparticles, slip velocity coefficient, Reynolds number and significant reduction in thermal resistance of solid wall, Nusselt number enhances. Behnampour et al. [18] analyzed heat transfer and nanofluid fluid flow in microchannels with trapezoidal-, rectangular- and triangular-shaped ribs. They found that for all studied Reynolds numbers, heat transfer values are least for rectangular rib. Therefore, trapezoidal-shaped ribs are recommended in high Reynolds numbers. Arabpour et al. [19] studied the heat transfer and laminar flow of kerosene/multi-walled carbon nanotubes (MWCNTs) nanofluid in the microchannel heat sink with slip boundary condition. They found that by increasing the slip velocity coefficient on the solid surfaces, the amount of minimum temperatures reduces significantly which behavior remarkably entails the heat transfer enhancement.

In this paper, laminar flow of water nanofluid/GNP–SDBS (graphene nanoplatelet–sodium dedecylbenzene sulfonate) for 0–0.1% solid nanoparticles mass fraction was studied for Reynolds numbers of 50–1000 in 3D space via finite volume method. In the new proposed microchannel design, the cooling fluid is moving in countercurrent in the upper and lower layers of the microchannels, and there are cavities and sinusoidal routes on the solid walls of the microchannel, and the presence of rectangular ribs on the flow centerline along the fluid path enhances mixing for cooling fluid and creates better heat transfer for warm surfaces.

Problem definition and mathematical method

Geometry

Using single-layer microchannels for heat transfer devices has been the topic of research by many researchers, and in most of the papers, the heat transfer behavior is fully investigated. In designing single-layer microchannel due to direct contact of microchannel wall with heat flux and the fact that the surfaces confining the fluid (inner walls of the microchannel) act as heat transfer surfaces, a nonuniform temperature distribution can occur. In order to fix this problem, increasing heat transfer surface is considered in

this study and the heat transfer and fluid flow behavior in the new microchannel for the double-layer microchannel configuration is considered. Figure 1 shows the new design of double-layer microchannel considered in this study. In this special design other than the structure of the double-layer microchannel, the sinusoidal cavities in the microchannel walls are used for disturbing thermal and velocity boundary layers at the walls. Also rectangular rips are used at microchannel center for improving fluid mixing in those regions. Based on Fig. 1, the fluid flow in the upper and lower layers passes in opposing directions. Also the microchannel in the upper layer and lower layers is separated by a silicon substrate with a thickness of W_{s} = 100 μm. The lower-layer microchannel is under the influence of constant heat flux of q'' = 50 W cm^{-2}, and the cool fluid in the upper and lower layers enters at T_{in} = 293.15 K. For improving heat transfer performance, GNP–SDBS (graphene nanoplatelet–sodium dodecylbenzene sulfonate) is used with mass fraction of 0, 0.02, 0.06 and 0.1% solid nanoparticles in water as base fluid. This investigation is done or Reynolds numbers of 50, 300, 700 and 1000 in 3D space and simulations are done with finite volume method.

This study is done on the 3D space in Cartesian coordinates. Based on Fig. 2-a, the coordinate system is placed at the bottom of silicon substrate and in the lower layer and in the center. In Fig. 2, parameters W_f and H_f are width and height of inlet and outlet sections for upper and lower layers of the microchannel which are the same for both layers. Parameters L_t and H_s are overall length and height of silicon substrate of the microchannel. Dimensions L_a and H_a are length and depth of sinusoidal cavities placed at microchannel walls. The considered microchannel has a thickness of silicon substrate equal to W_s = 100 μm, and this thickness is constant for microchannel walls. The dimensions L_r and W_p are length and height of ribs placed in the microchannel center, respectively.

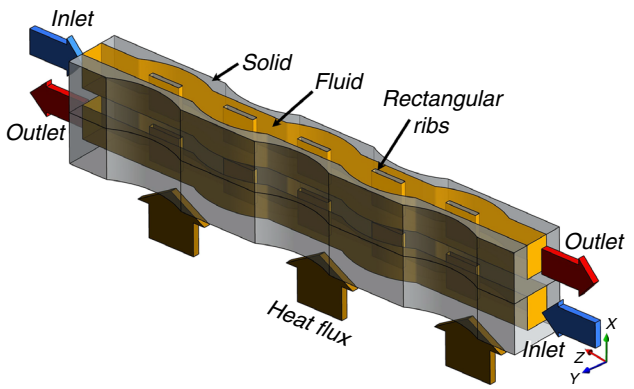

Fig. 1 New design of two-layer microchannel considered in this study

Also, the upper layer of the microchannel is considered without thickness and insulated. The precise dimensions introduced for microchannel geometry are given in Table 1. The precise dimensions in Fig. 2 are according to values in Table 1. Also, all of the dimensions have micrometer units.

In this numerical study, nanofluid flow and heat transfer are simulations in laminar flow and 3D space in Cartesian coordinates. The nanofluid properties are considered to be constant and independent of temperature. The solid–liquid suspension is simulation in mass fractions of 0–0.1% as single phase and Newtonian.

A constant heat flux is imposed on the microchannel walls. The no-slip boundary condition is applied on microchannel walls. The nanofluid behavior in the considered mass fractions is considered to be Newtonian. The effects of dispersion and thermophoresis are neglected. The effect of gravity acceleration is negligible, and the fluid flow is completely forced.

Numerical approach

Continuity equation

$$\frac{\partial u}{\partial x}+\frac{\partial v}{\partial y}+\frac{\partial w}{\partial z}=0. \tag{1}$$

Momentum equation

$$u\frac{\partial u}{\partial x}+v\frac{\partial u}{\partial x}+w\frac{\partial u}{\partial x}=-\frac{1}{\rho_{nf}}\frac{\partial p}{\partial x} + \nu_{nf}\left(\frac{\partial}{\partial x}\left(\frac{\partial u}{\partial x}\right)+\frac{\partial}{\partial y}\left(\frac{\partial u}{\partial y}\right)+\frac{\partial}{\partial z}\left(\frac{\partial u}{\partial z}\right)\right). \tag{2}$$

$$u\frac{\partial v}{\partial x}+v\frac{\partial v}{\partial y}+w\frac{\partial v}{\partial z}=-\frac{1}{\rho_{nf}}\frac{\partial p}{\partial y} + \nu_{nf}\left(\frac{\partial}{\partial x}\left(\frac{\partial v}{\partial x}\right)+\frac{\partial}{\partial y}\left(\frac{\partial v}{\partial y}\right)+\frac{\partial}{\partial z}\left(\frac{\partial v}{\partial z}\right)\right). \tag{3}$$

$$u\frac{\partial w}{\partial x}+v\frac{\partial w}{\partial y}+w\frac{\partial w}{\partial z}=-\frac{1}{\rho_{nf}}\frac{\partial p}{\partial z} + \nu_{nf}\left(\frac{\partial}{\partial x}\left(\frac{\partial w}{\partial x}\right)+\frac{\partial}{\partial y}\left(\frac{\partial w}{\partial y}\right)+\frac{\partial}{\partial z}\left(\frac{\partial w}{\partial z}\right)\right). \tag{4}$$

Energy equation

$$u\frac{\partial T}{\partial x}+v\frac{\partial T}{\partial y}+w\frac{\partial T}{\partial z} =\frac{1}{\rho_{nf}C_{p,nf}}\frac{\partial}{\partial x}\left(\left(K_{nf}\frac{\partial T}{\partial x}\right)+\frac{\partial}{\partial y}\left(K_{nf}\frac{\partial T}{\partial y}\right)+\frac{\partial}{\partial z}\left(K_{nf}\frac{\partial T}{\partial z}\right)\right). \tag{5}$$

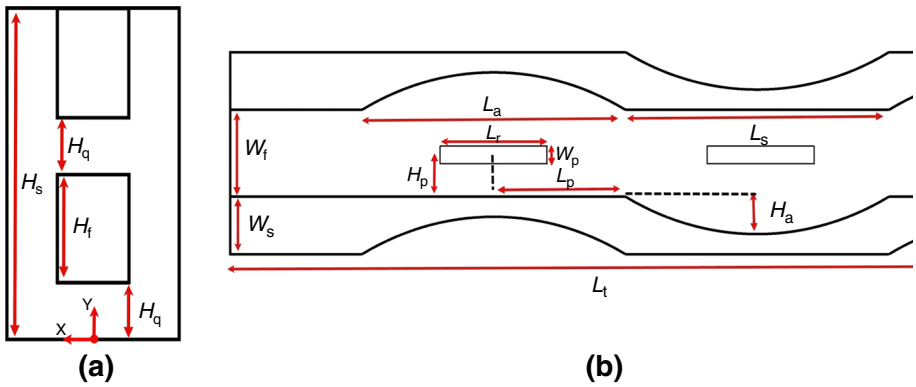

Fig. 2 Introducing parametric dimensions for the considered geometry

Table 1 Precise dimensions of the considered geometry in this study

Parameter	Value/μm	Parameter	Value/μm
W_f	150	L_a	500
W_s	100	L_s	500
W_p	30	L_r	200
H_f	200	L_p	250
H_s	600	L_t	3000
H_a	65	H_q	100
H_p	75	–	–

Boundary conditions

Normal uniform distribution of temperature and velocity is applied for fluid at the channel. In addition, zero relative pressure is employed at the channel outlets. A no-slip condition is utilized at the interface of walls and fluid. Moreover, a constant heat flux (50 W cm^{-2}) is applied on the bottom of down channel, and the temperature of the inlet is considered 293.15 K for the outer solid walls, and the symmetry condition is considered. Moreover, the temperature of nanofluid is equal wall temperature at the interface of wall and base fluid.

Table 2 summarizes the thermophysical properties of water nanofluid/GNP–SDBS which is calculated by Arzani et al. [20], employed in the current research.

CFD simulation, mesh study and validation

Although the relative error of numerical prediction in comparison with experimental results is not low, due to high cost of experimental platform for any case, recently, the tendency of researchers toward using numerical method instead of experimental approach is elevated [21–25].

Discretization of the nonlinear differential equations is carried out by the finite volume approach using the second-order upwind method [26–28]. To couple the velocity and pressure, the SIMPLE [29, 30] scheme is employed. Moreover, the convergence criterion is considered 10^{-6} for the relative residuals related to all parameters [31, 32]. The structured meshes with uniform grid are applied for both domains (fluid and solid) according to Fig. 3. The assumptions used during simulation are as follows: single-phase approach for simulation of fluid, steady and Newtonian fluid flow, temperature independent for nanofluid characteristic, no-slip condition on interface of fluid and solid domain and symmetry condition on the outer solid wall.

For grid independency, the average Nusselt number is calculated with different cell numbers. The results of mesh study are presented in Table 3. As can be observed, by increasing the number of grids, the difference percentage of Nusselt numbers decreases and no significant change is noticed in the Nusselt number for the grids with the cell number higher than 428,600.

Hence, these grids are selected to investigate the nanofluid flow in these geometries.

For verification of simulated results, the numerical predictions are compared with experimental results reported by Wei et al. [33] which showed wall temperature of double-layer microchannel with rectangular cross section, 83 mL min^{-1} mass flow rate for each Layer, water inlet temperature at 20 °C and 71 w cm^{-2} for uniform constant heat flux at the bottom on microchannel. The experimental platform was involved two channels with 1.8 mm and 1 mm as length and 284 μm × 56 μm and 243 μm × 56 μm for upper and lower layers, respectively. According to Table 4, the numerical predictions are in a good agreement with the considered experimental work. (Maximum relative error is higher than 1 °C.) Therefore, it can be noted that the numerical approach is valid.

Table 2 Thermophysical properties of nanofluid

Thermophysical properties	Water	0.02%	0.06	% 0.10%
Thermal conductivity/$Wm^{-1}K^{-1}$	0.6230	0.6450	0.675	0.695
Viscosity/Pa s	0.0007	0.0010	0.0011	0.0013
Density/kg m^{-3}	994.1	995.1151	996.8895	998.158
Specific heat capacity/J Kg^{-1} K^{-1}	4178	4152.66	4104.075	4055.95

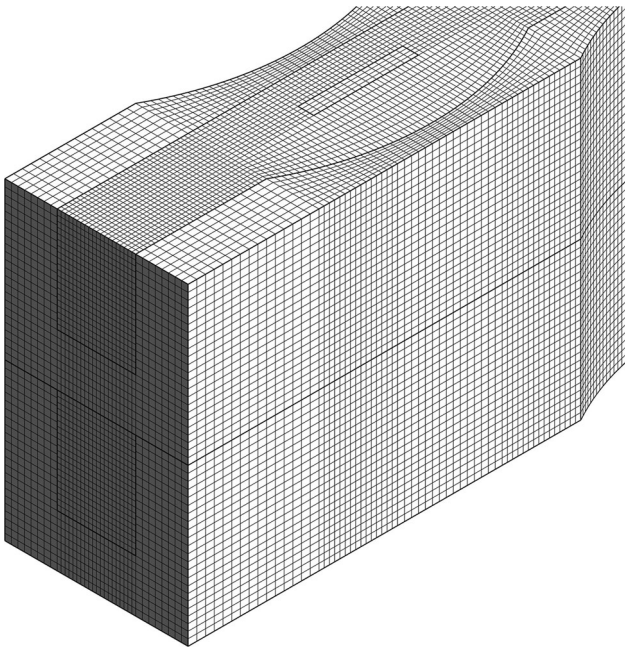

Fig. 3 The grid type used in this study

Table 3 Mesh study results for Re = 50, ϕ = 0.00% (water)

Elements number	Nusselt number	Percentage of difference
391,720	18.967	9.880
397,364	20.841	3.450
425,380	21.56	2.156
428,600	22.025	0.0136
437,240	22.028	Base mesh

Data reduction

The Nusselt number (Nu) is calculated through the following equation [34]:

$$Nu = \frac{hD}{k}, \tag{6}$$

where h and D denote the convective heart transfer coefficient and hydraulic diameter, which are obtained as follows [35]:

$$D = \frac{4A}{P}, \tag{7}$$

$$h = \frac{q''}{\bar{T}_s - T_m}, \tag{8}$$

where $\bar{T}_s$ is the average wall temperature of the bottom wall, q" denotes the wall heat flux, Tm indicates the mean temperature of the fluid and A and $P$are cross-sectional area and wetted perimeter of the cross section, respectively. In order to calculate the friction factor (f), Darcy friction factor is used, according to Eq. (9) [36].

$$f = \frac{2D\Delta P}{L\rho U_m^2}, \tag{9}$$

where L, D and U_m represent the channel length, the hydraulic channel diameter and the cross-sectional area-weighted average of the flow velocity, respectively. Also, ΔP indicates the average of bottom and upper channels of pressure drop. The main purpose of applying nanofluid is to improve the Nusselt number. However, the use of nanofluids also increases the friction factor and pumping power. Hence, a parameter called performance evaluation criteria (PEC) is defined here to examine overall thermo-hydraulic performance. This parameter shows the enhancement of Nusselt number in comparison with that of pressure drop, when nanoparticles are injected into a tube. It is defined as follows [37]:

$$PEC = \frac{Nu/Nu_0}{(f/f_0)^{1/3}}, \tag{10}$$

where Nu_0 and ΔP_0 are the Nusselt number and pressure drop of the base fluid, respectively.

The amount of thermal resistance at the bottom wall of microchannel is calculated by [38]:

$$R = \frac{T_{max} - T_{in}}{q'' \times A_{bottom}}, \tag{11}$$

where T_{max}, T_{in}, A and q'' wall are, respectively, the maximum temperature of bottom wall, minimum temperature which is the inlet temperature of fluid, cross-sectional area of applied heat flux and applied heat flux on the bottom wall.

Table 4 Comparisons between numerical and experimental results

Distance from inlet (m)	Temperature/K		
	Experimental data [33]	Numerical prediction	Error
0.0005	306.182	305.4607	2.36E − 01
0.0015	308.6	308.0666	1.73E − 01
0.003	310.909	310.9394	9.78E − 03
0.004	312.364	312.3074	1.81E − 02
0.005	313.164	313.3398	5.61E − 02
0.006	313.564	314.1134	1.75E − 01
0.007	313.309	314.6955	4.41E − 01
0.008	313.164	315.1436	6.28E − 01
0.009	312.454	315.5057	9.67E − 01

Results and discussion

In Fig. 4, the graphs of variations of average Nusselt number are shown for Reynolds numbers of 50, 300, 700 and 1000 for different solid nanoparticles mass fractions which are dissolved in water. Based on this figure, the increase in fluid velocity (Reynolds number) has a significant effect on increasing convective heat transfer ratio of cooling fluid in the considered geometry, so that by increasing Reynolds number of the fluid, the Nusselt number is increased significantly. Increasing solid nanoparticles in the base fluid improves heat conduction of the cooling fluid and improves temperature distribution between different fluid layers, and this behavior reduces temperature gradients in the cooling fluid. For different considered nanoparticle mass fractions in the base fluid, it can be said that the variations of increasing Nusselt number for Reynolds number of 50 have a lower distinction compared with other Reynolds numbers. The use of solid nanoparticles for mass fractions of 0.02, 0.04 and 0.1 can have a clear effect on increasing Nusselt number for Reynolds numbers of 300 and 700. For Reynolds number of 1000, increasing mass fraction of solid nanoparticles in the base fluid does not make any changes in increasing Nusselt number and this behavior can be due to negative impacts of adding solid nanoparticles in a special mass fraction or higher mass fractions or the selection of Newtonian fluid model for approximating flow field and heat transfer in the given mass fraction might not be a good model. Curves in Fig. 5 show the Darcy friction factor for Reynolds number of 50–1000 for mass fractions of 0, 0.02, 0.04 and 0.1% solid nanoparticles. This factor is dependent on increasing fluid pressure drop in the microchannel path and value of average inlet velocity for each of the different

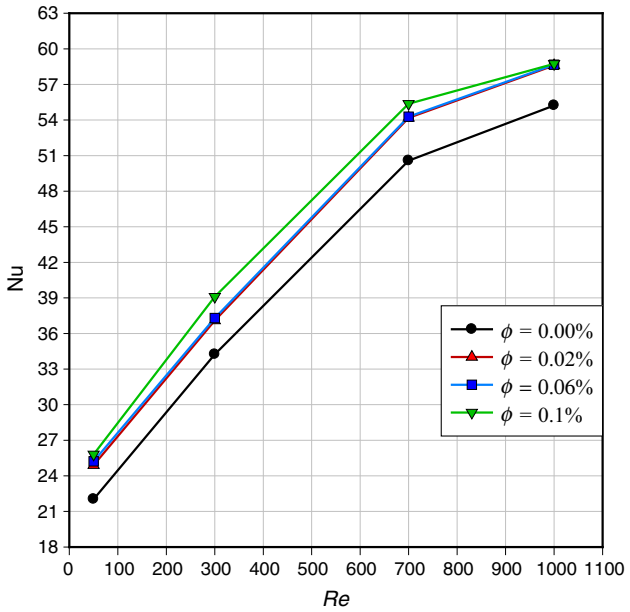

Fig. 4 Changes in average Nusselt number for different Reynolds numbers and different solid nanoparticles mass fractions

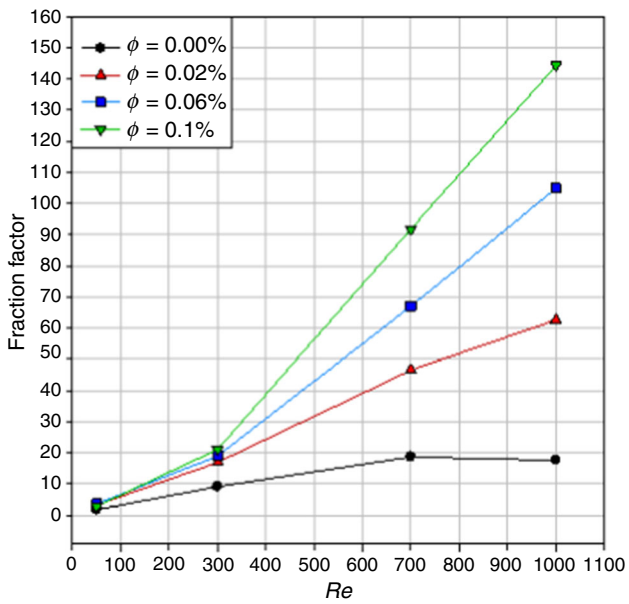

Fig. 5 Darcy friction factor for Reynolds number in the range 50–1000 for different solid nanoparticles mass fractions

Reynolds number parameters and mass fractions. By increasing fluid velocity due to placement of ribs in the center and cavities on the microchannel walls, strong velocity gradients are formed and the fluid in the longitudinal path and in some areas due to surface features will have secondary flows, especially in high Reynolds numbers. These features reduce kinetic energy of the fluid in motion and change them to pressure drop.

By increasing fluid momentum (higher Reynolds number), the formation of secondary flows and changes in direction of fluid components is increased. Therefore, by increasing Reynolds number the level of friction factor curves is significantly increased. Increasing solid nanoparticles mass fraction based on the given properties in this study causes an increase in density and viscosity of the cooling fluid. By increasing viscosity of the cooling fluid, the effect of shear stress on the fluid motion, especially in regions close to wall, becomes significant and these effects have a more prominent effect by further movement of fluid toward outlet section, while moving to central regions of the flow and because of an increase in friction factor and momentum dissipation increase, their effect becomes significant.

Also by increasing cooling fluid density, the fluid motion and convection in the microchannel, especially in sinusoidal cavities, will require higher energy; as a result, this behavior results in higher momentum dissipation and fluid kinetic energy loss in higher solid nanoparticles mass fraction and increasing the level of friction factor curves are seen consequently. In general, employing the new microchannel design with sinusoidal cavities in solid walls and placement of ribs in the central flow regions results in better flow mixing and increases Nusselt number; on the other hand, it increases Darcy friction factor and this behavior is more prominent by increasing Reynolds number.

In Fig. 6, the effect of Reynolds number variations and using nanofluid with different mass fractions on the thermal resistance behavior of the solid wall for the bottom of the lower layer of the microchannel is considered. Thermal resistance is an important factor which considers the effects of flow and geometric parameters on the cooling performance of solid walls of the microchannel (decrease in maximum temperature in the lower microchannel layer). Parameters such as increasing Reynolds number and solid nanoparticles mass fraction result in increased Nusselt number which reduces maximum temperature in the lower layer of the microchannel and reduces thermal resistance. On the other hand, the meaning of reducing thermal resistance is that any agent that creates uniform temperature distribution in the microchannel can eliminate temperature gradients and hot zones and reduces maximum temperature of the microchannel solid walls. Also

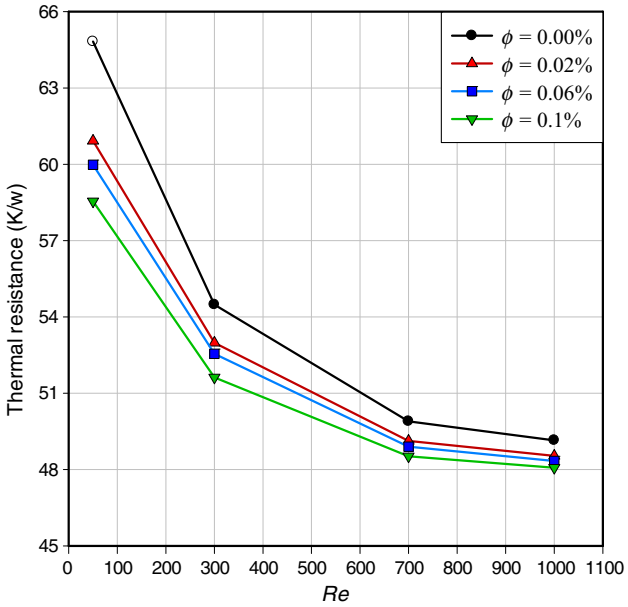

Fig. 6 Changes in thermal resistance of the solid wall for the bottom of the lower layer of the microchannel

decreasing thermal resistance of the lower microchannel wall in lower Reynolds number is dependent of increasing solid nanoparticles mass fraction and the dependence is strong. The distinction in behavior related to decreasing thermal resistance of the warm wall of the microchannel for Reynolds number of 1000 has a smaller effect for different mass fractions so that decreasing maximum temperature of the bottom wall of the microchannel tends to a constant value by increasing Reynolds number and solid nanoparticles mass fraction. Based on the behavior of thermal resistance graphs, the lowest value of this factor happens for Reynolds number of 1000 and solid nanoparticles mass fraction of 0.1%.

In Fig. 7, the thermal efficiency curves for different Reynolds numbers and solid nanoparticles mass fractions are compared. The thermal efficiency factor is the ratio of an increase in Nusselt number divided by an increase in friction coefficient for each mass fraction compared with the base fluid. This investigation is done for each Reynolds number compared with the similar cases. The trends of thermal efficiency are influenced by heat transfer, and changes in friction factor show different behaviors for Reynolds numbers of 50, 300, 700 and 1000. Adding the solid nanoparticles mass fraction, presence of sinusoidal cavities and counterflow in the upper and lower layers of the channel has an effect on temperature field and flow structure and creates complete mixing for all of the regions of the microchannel along fluid route. Based on the considered factors for increasing heat transfer, and the magnitude of its effect on increasing friction factor, it can have different behaviors. In curves of Fig. 7, adding solid

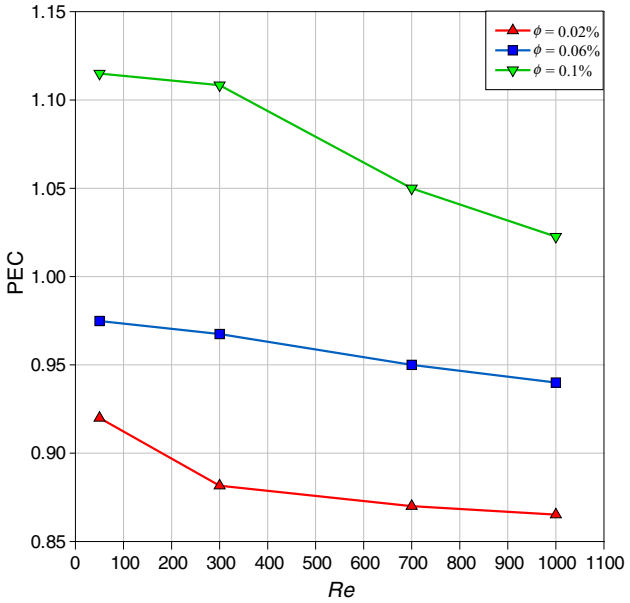

Fig. 7 Thermal efficiency curves for different Reynolds numbers and solid nanoparticles mass fractions

nanoparticles mass fraction results in increased Nusselt number and improved thermal efficiency factor and the level of the curves for this factor has shown a good trend for all solid nanoparticles mass fractions. The presence of sinusoidal cavities on the walls of the microchannel and rectangular ribs in the microchannel center has a good effect on increasing Nusselt number, but according to friction factor curves, it causes a significant increase in friction factor values, and this will result in decreasing trend of thermal efficiency curves by increasing Reynolds number.

In general, the best compromise between Nusselt number performance and friction factor happens for Reynolds number of 50 and solid nanoparticles mass fraction of 0.1%. By increasing Reynolds number, the effect of increasing friction factor compared with Nusselt number will become dominant and result in decreasing trend of thermal efficiency curves.

In bar charts of Fig. 8, the average static temperature in the outlet sections of the upper and lower layers of the microchannel is compared for Reynolds number of 50–1000 and mass fraction of 0–0.1% solid nanoparticles. During entrance of cooling fluid with lower temperature, heat exchange happens between fluid and walls and the warm temperature of the walls penetrates into the fluid. By further movement of fluid into the microchannel, the effects of heat penetration in the central areas of the flow become pronounced. Due to an increase in temperature of the fluid, the value of heat transfer is reduced. The reason for this behavior is an increase in fluid temperature and a decrease in temperature difference between cooling fluid and warm surfaces. Also factors such as sinusoidal cavities and ribs placed in the channel improve flow mixing and elimination of hot fluid zones at the neighborhood of solid walls. Also increasing solid nanoparticles mass fraction results in more uniform temperature distribution between fluid layers. By slow movement of fluid in Reynolds number of 50, the penetration of heat from warm walls to different cooling fluid zones is increased and heat transfer between fluid and warm surface is reduced. By increasing fluid velocity, the value of convective heat transfer is elevated and the temperature of the inlet fluid compared with the penetrated heat into the microchannel becomes dominant. As a result, by increasing Reynolds number the average temperature of the outlet section is reduced. Also among the considered cases the highest average outlet temperature was observed for pure water fluid, and by increasing solid nanoparticles mass fraction, the value of fluid temperature in the outlet section is significantly reduced which can improve heat transfer. In general factor such as increased fluid velocity, an increase in solid nanoparticles mass fraction causes an increase in convective heat transfer in the microchannel and results in domination of inlet fluid temperature in the microchannel and a reduction in heat penetration into fluid layers.

In bar charts of Fig. 9, the average static pressure drop for outlet sections in the upper and lower layers of the microchannel for different Reynolds numbers and solid nanoparticles mass fractions is compared. By movement of fluid in the microchannel and contact of fluid with solid walls, the effects of surface shear stress on the fluid layers are increased and some part of the fluid kinetic energy is lost.

Also factors such as presence of sinusoidal cavities in the walls of the considered geometry and presence of ribs at flow center cause changes in the components of fluid velocity and result in formation of secondary flows in different flow regions, and this behavior has a high effect on dissipating kinetic energy of the cooling fluid and a large portion of the kinetic energy of the fluid is converted to pressure drop. By increasing fluid velocity, the above-mentioned effects about decreasing fluid momentum become stronger and the pressure drop becomes more significant. For low Reynolds number (Reynolds of 50 and 300) due to lower fluid velocity, the fluid can adapt to surfaces better and the presence of surface features for flow mixing will have a smaller effect on increasing pressure drop. Therefore, the level of pressure drop curves for these Reynolds numbers is lower compared with Reynolds numbers of 700 and 1000. Increasing pressure drop for Reynolds numbers of 700 and 1000 is mainly because of presence of fluid mixing features on the surface such as presences of cavities and ribs, and by increasing solid nanoparticles mass fraction, then the level of pressure drop

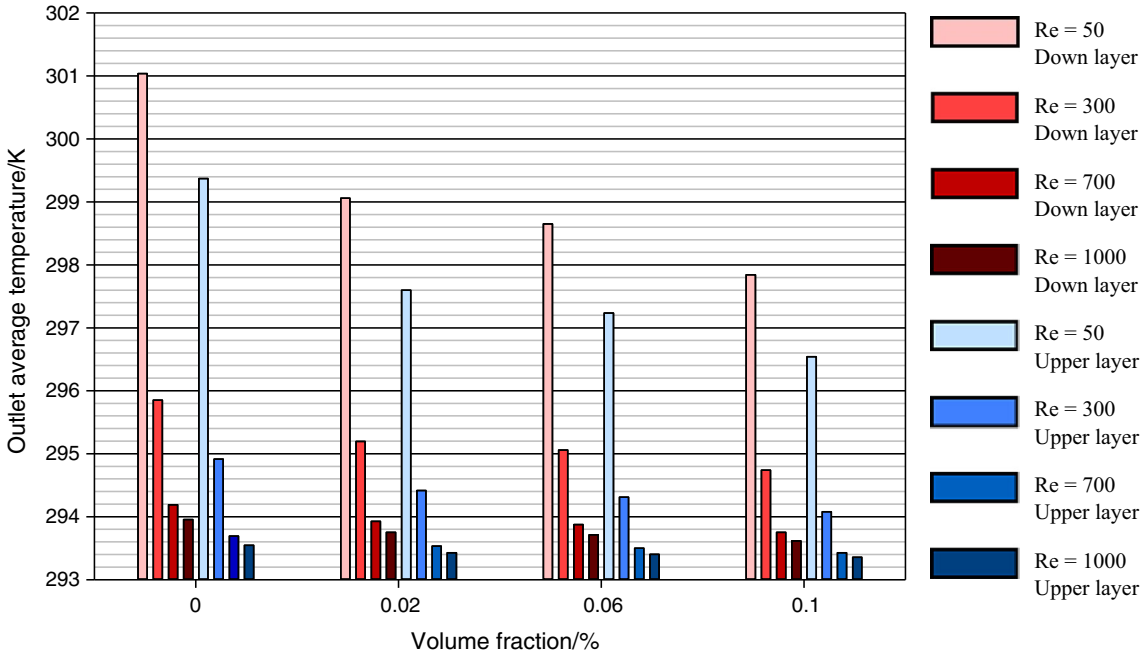

Fig. 8 Average static temperature in the outlet section for the upper and lower layers of the microchannel

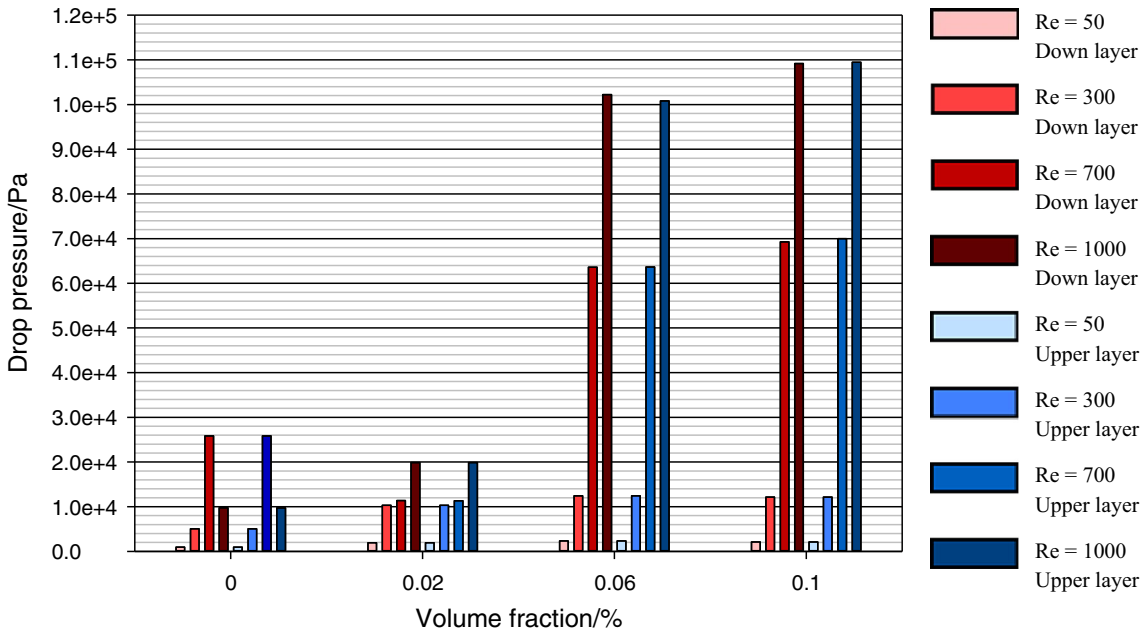

Fig. 9 Average static pressure drop for outlet sections for upper and lower layers of the microchannel

will increase significantly. Based on the behavior of the graph, the implementation of the mentioned geometry for high Reynolds numbers is good for mass fraction lower than 0.06% and for mass fractions of 0.06 and above the value of pressure drop in the microchannel is significant.

Contours of static temperature distribution are shown in Fig. 10 for section $Y = 0$ for solid nanoparticles mass fraction of 0.02% for Reynolds numbers of 50, 300, 700 and 1000. In these contours, the distribution of static temperature in the longitudinal flow plane and in different regions such as regions behind and in front of ribs for upper and lower layers is clearly exhibited. The presence of surface features which result in flow mixing has a high effect on uniform distribution of heat in the microchannel. But according to the flow direction in the upper and lower layers in the regions behind the ribs along flow route due to

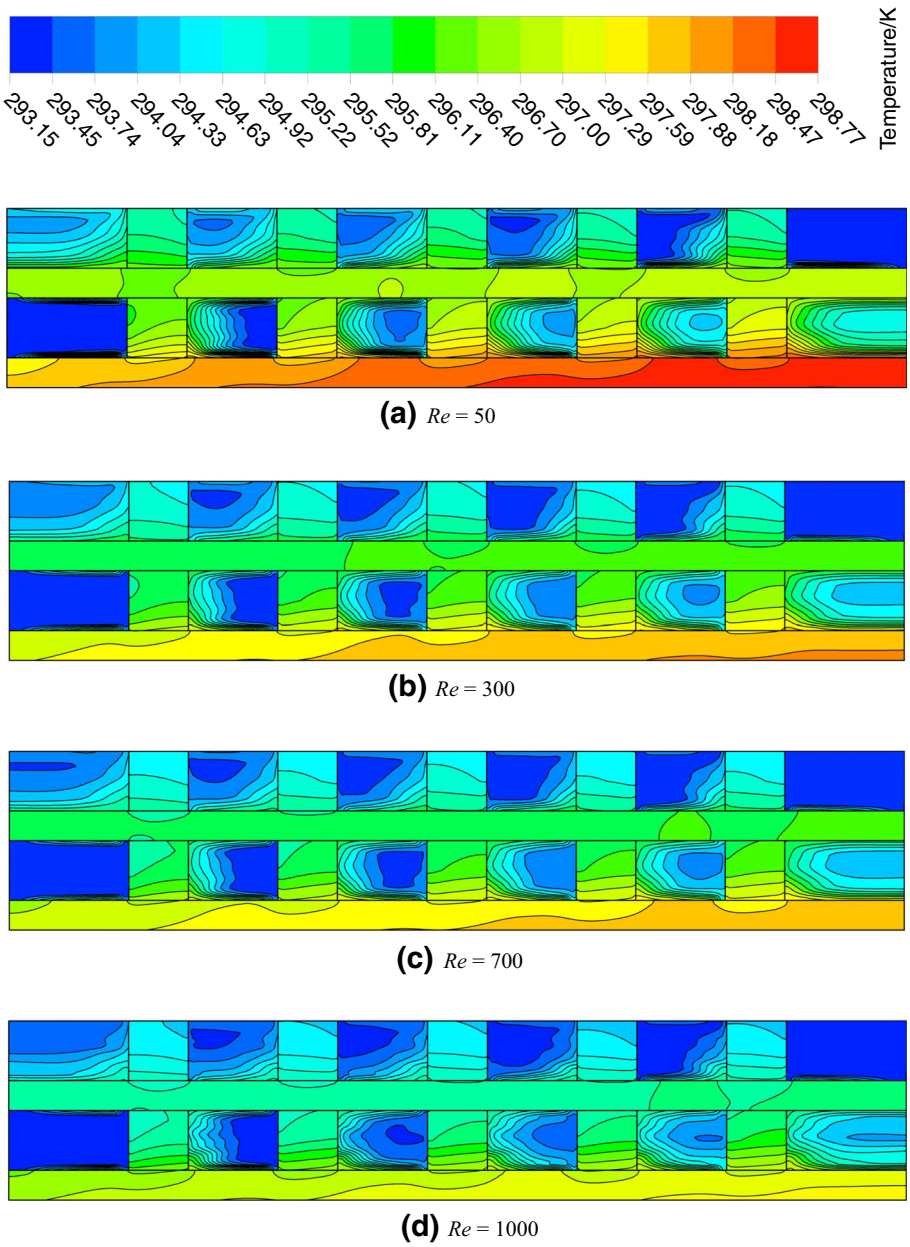

Fig. 10 Static temperature/K distribution contours for $Y = 0$ section for solid nanoparticles mass fraction of 0.02%

presence of separation zones and formation of vortices, the value of heat transfer in these areas is not uniform similar to other parts of the microchannel and in these areas zones with lower heat transfer (hot zones) area created. Also the bottom of the lower layer of the microchannel has direct contact with the constant heat flux and therefore has the highest temperature and temperature gradients which are obvious in the figure. In the lower layer of the microchannel and the beginning of the inlet section due to temperature difference between fluid and wall, the value of heat transfer is elevated and the temperature of the inlet fluid is dominant and these areas are colder. By further progression of fluid into the microchannel, the value of heat transfer is reduced and hot zones are formed in the lower layer. By increasing Reynolds number, the temperature distribution in the lower layer is reduced because of an increase in heat transfer and the position of maximum temperature moves toward the outlet section.

Contours of static temperature for the lower layer (y = 150 μm plane) and the upper microchannel layer (y = 450 μm plane) longitudinally along the flow for different Reynolds numbers and solid nanoparticles mass fraction of 0.02% are investigated in Fig. 11. By movement of fluid in the microchannel, the effect of heat penetration from warm walls to central areas of the flow will become significant by further progression of fluid toward outlet section for the lower and upper layers of the microchannel. The presence of sinusoidal cavities on the solid walls and

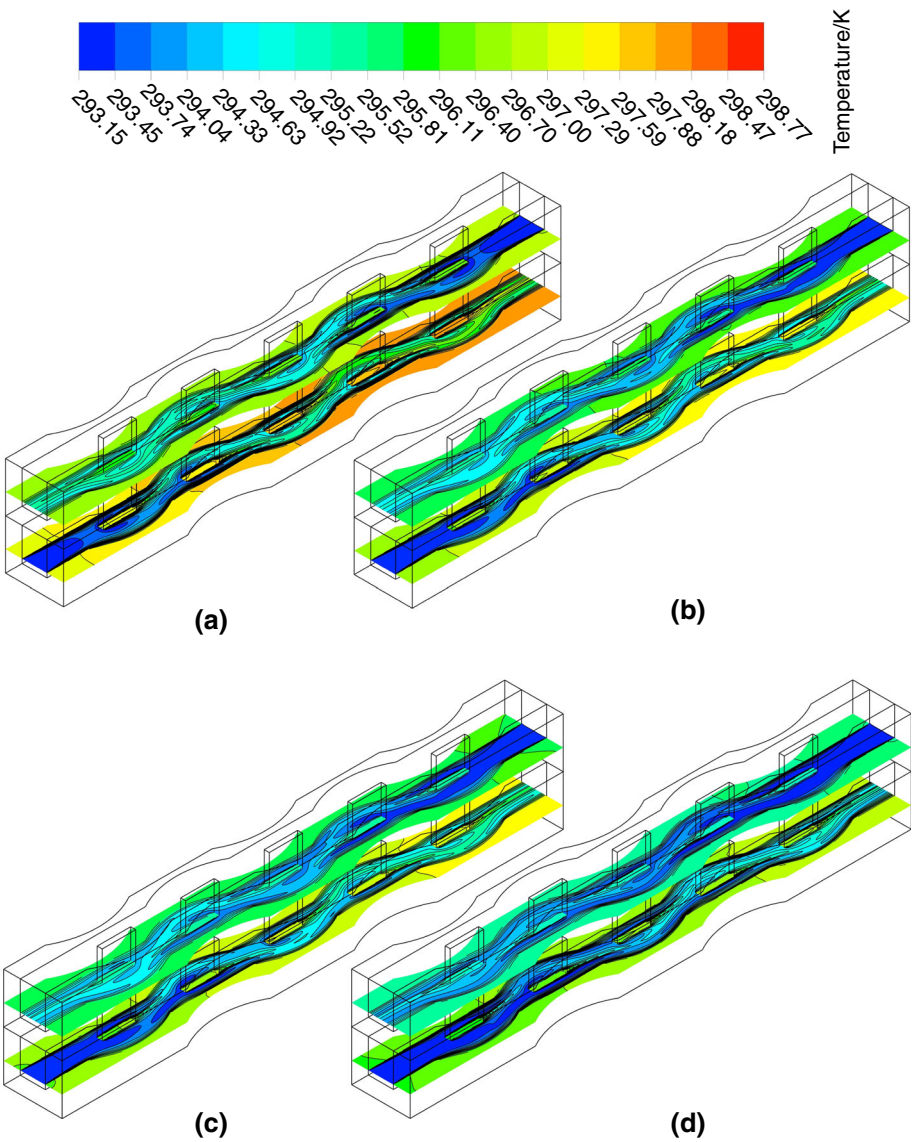

Fig. 11 Static temperature/K contours for plane y = 150 μm and y = 450 μm along the length of the microchannel for different Reynolds numbers and solid nanoparticles mass fraction of 0.02%. **a** Re = 50, **b** Re = 300, **c** Re = 700, **d** Re = 1000

presence of rectangular ribs in the flow centerline (ribs) improve mixing and enhance temperature distribution of the fluid in different longitudinal sections of the microchannel. Due to behavior of temperature contours in Fig. 11, because the lower layer is in direct contact with the heat flux, the highest effect due to presence of temperature gradients on solid walls and cooling fluid happens in the lower layer. In the upper layer due to weaker and indirect contact with the warm wall of the microchannel for all of the considered Reynolds number, a more uniform temperature distribution is obtained. In general, for geometries for fluid mixing features such as sinusoidal cavity and ribs along fluid route, because of better mixing and disturbance of thermal and velocity boundary layers, in higher velocities the temperature distribution is more uniform and hot zones are largely eliminated for high Reynolds numbers such as 700 and 1000.

Conclusions

In this numerical study, the simulation of water nanofluid–GNP–SDBS for mass fraction of 0–0.1% for a new microchannel heat sink design with two layers in the presence of sinusoidal cavities was carried out. The numerical study was done for laminar Reynolds numbers for range of 50, 300, 700 and 1000, and the numerical simulation was conducted with finite volume method in 3D space. In this study, the use of fluid mixing factors in the new microchannel design by application of nanofluid as a suitable and highly efficient tool was studied. The application of nanofluid, according to previous studies [39–49], has had a significant contribution toward improving heat transfer of the new design of the microchannel by increasing heat conduction of the nanofluid and micron-scale mechanisms of heat transfer, and on the other hand,

by increasing Reynolds number, because of reinforcement of convective heat transfer coefficient, this behavior is amplified. Among the considered Reynolds numbers, the Reynolds numbers of 1000, 700, 300 and 50 have the highest and lowest Nusselt number values, respectively. The presence of ribs in the microchannel improves heat transfer and causes a sharp rise in friction factor and pressure drop in the microchannel. The above behavior shows a significant increase for Reynolds numbers of 1000 and 700 which is because of intense variations of velocity gradients and fluid momentum dissipation in high Reynolds numbers because of application of these devises in the microchannel. Also by increasing viscosity of the cooling fluid, the effects of shear stress due to movement of fluid on the solid walls, especially in areas close to wall, become significant and these effects are transferred to central areas of the flow upon further movement of fluid toward exit section and have a contribution in raising friction factor and increasing momentum dissipation. By increasing density of cooling fluid (solid nanoparticles mass fraction), the motion of the fluid and convection of fluid in the microchannel especially in the sinusoidal cavities will require higher energy; as a result, this behavior results in higher fluid momentum and kinetic energy dissipation in higher solid nanoparticles mass flow rates and will result in elevation of level of curves related to friction factor. Any feature that can cause a uniform distribution of heat in the microchannel can eliminate temperature gradients and warm zones and will reduce maximum temperature in the solid wall of the microchannel. Because of direct contact of lower layer with the heat flux, the highest effect of presence of temperature gradients on solid walls and cooling fluid happens in the lower layer. In the upper layer because of weaker and indirect contact with the warm wall of the microchannel, for all of the considered Reynolds numbers, a more uniform temperature distribution is observed. In general, the new investigation design can improve heat transfer efficiency significantly and reduction in effects such as pressure drop and friction factor can be achieved by using different rib designs which provide less blockage against the flow.

References

1. Heydari A, Akbari OA, Safaei MR, Derakhshani M, Alrashed AA, Mashayekhi R, Shabani GA, Zarringhalam M, Nguyen TK. The effect of attack angle of triangular ribs on heat transfer of nanofluids in a microchannel. J Therm Anal Calorim. 2018;131(3):2893–912.
2. Gholami MR, Akbari OA, Marzban A, Toghraie D, Shabani GA, Zarringhalam M. The effect of rib shape on the behavior of laminar flow of oil/MWCNT nanofluid in a rectangular microchannel. J Therm Anal Calorim. 2017. https://doi.org/10.1007/s10973-017-6902-3.
3. Karimipour A, Alipour H, Akbari OA, Semiromi DT, Esfe MH. Studying the effect of indentation on flow parameters and slow heat transfer of water-silver nano-fluid with varying volume fraction in a rectangular two-dimensional micro channel. Ind J Sci Tech. 2015. https://doi.org/10.17485/ijst/2015/v8i15/51707.
4. Safaei MR, Gooarzi M, Akbari OA, Shadloo MS, Dahari M. Performance evaluation of nanofluids in an inclined ribbed microchannel for electronic cooling applications. In: Electronics cooling 2016. InTech.
5. Parsaiemehr M, Pourfattah F, Akbari OA, Toghraie D, Sheikhzadeh G. Turbulent flow and heat transfer of Water/Al2O3 nanofluid inside a rectangular ribbed channel. Physica E. 2018;96:73–84.
6. Bahmani MH, Sheikhzadeh G, Zarringhalam M, Akbari OA, Alrashed AA, Shabani GA, Goodarzi M. Investigation of turbulent heat transfer and nanofluid flow in a double pipe heat exchanger. Adv Powder Technol. 2018;29(2):273–82.
7. Ahmadi AA, Khodabandeh E, Moghadasi H, Malekian N, Akbari OA, Bahiraei M. Numerical study of flow and heat transfer of water-Al2O3 nanofluid inside a channel with an inner cylinder using Eulerian-Lagrangian approach. J Therm Anal Calorim. 2018;132:651–65.
8. Hosseinnezhad R, Akbari OA, Afrouzi HH, Biglarian M, Koveiti A, Toghraie D. Numerical study of turbulent nanofluid heat transfer in a tubular heat exchanger with twin twisted-tape inserts. J Therm Anal Calorim. 2018;132(1):741–59.
9. Akbari OA, Afrouzi HH, Marzban A, Toghraie D, Malekzade H, Arabpour A. Investigation of volume fraction of nanoparticles effect and aspect ratio of the twisted tape in the tube. J Therm Anal Calorim. 2017;129(3):1911–22.
10. Lin L, Chen YY, Zhang XX, Wang XD. Optimization of geometry and flow rate distribution for double-layer microchannel heat sink. Int J Therm Sc. 2014;78:158–68.
11. Sakanova A, Yin S, Zhao J, Wu JM, Leong KC. Optimization and comparison of double-layer and double-side micro-channel heat sinks with nanofluid for power electronics cooling. Appl Therm Eng. 2014;65(1–2):124–34.
12. Mohebbi K, Rafee R, Talebi F. Effects of rib shapes on heat transfer characteristics of turbulent flow of Al2O3-water nanofluid inside ribbed tubes. Iran J Chem Chem Eng. 2015;34(3):61–77.
13. Akbari OA, Toghraie D, Karimipour A. Impact of ribs on flow parameters and laminar heat transfer of water–aluminum oxide nanofluid with different nanoparticle volume fractions in a three-dimensional rectangular microchannel. Adv Mech Eng. 2015;7(11):1–11.
14. Leng C, Wang XD, Wang TH. An improved design of double-layered microchannel heat sink with truncated top channels. Appl Therm Eng. 2015;79:54–62.
15. Wang H, Chen Z, Gao J. Influence of geometric parameters on flow and heat transfer performance of micro-channel heat sinks. Appl Therm Eng. 2016;107:870–9.
16. Osanloo B, Mohammadi-Ahmar A, Solati A, Baghani M. Performance enhancement of the double-layered micro-channel heat sink by use of tapered channels. Appl Therm Eng. 2016;102:1345–54.
17. Arabpour A, Karimipour A, Toghraie D, Akbari OA. Investigation into the effects of slip boundary condition on nanofluid flow in a double-layer microchannel. J Therm Anal Calorim. 2018;131(3):2975–91.
18. Behnampour A, Akbari OA, Safaei MR, Ghavami M, Marzban A, Shabani GA, Mashayekhi R. Analysis of heat transfer and nanofluid fluid flow in microchannels with trapezoidal, rectangular and triangular shaped ribs. Physica E. 2017;91:15–31.

19. Arabpour A, Karimipour A, Toghraie D. The study of heat transfer and laminar flow of kerosene/multi-walled carbon nanotubes (MWCNTs) nanofluid in the microchannel heat sink with slip boundary condition. J Therm Anal Calorim. 2018;131(2):1553–66.
20. Arzani HK, Amiri A, Kazi SN, Chew BT, Badarudin A. Experimental and numerical investigation of thermophysical properties, heat transfer and pressure drop of covalent and noncovalent functionalized graphene nanoplatelet-based water nanofluids in an annular heat exchanger. Int Commun Heat Mass. 2015;68:267–75.
21. Li K, Wright, J, Modaresahmadi S, Som D, Williams W, Bird JZ. Designing the first stage of a series connected multistage coaxial magnetic gearbox for a wind turbine demonstrator. In Energy conversion congress and exposition (ECCE), 2017 IEEE (pp 1247–1254). IEEE
22. Khalesi J, Modaresahmadi S, Atefi G. SEM Gamma prime observation in a thermal and stress analysis of a first-stage Rene'80H gas turbine blade: numerical and experimental investigation. Iran J Sci Technol Trans Mech Eng. 2018. https://doi.org/10.1007/s40997-018-0235-0.
23. Ahmadi SM, Ghazavi MR, Sheikhzad M. Dynamic analysis of a rotor supported on ball bearings with waviness and centralizing springs and squeeze film dampers. Int J Eng Trans C. 2015;28(9):1351–8.
24. Som D, Li K, Kadel J, Wright J, Modaresahmadi S, Bird JZ, William W. Analysis and testing of a coaxial magnetic gearbox with flux concentration halbach rotors. IEEE Trans Magn. 2017;53(11):1–6.
25. Wong HY, Bird JZ, Modaresahmadi S, Williams W. Comparative analysis of a coaxial magnetic gear with a flux concentration rotor and consequent pole rotor typology. IEEE Trans Magn. 2018;99:1–5.
26. Akbari OA, Toghraie D, Karimipour A. Numerical simulation of heat transfer and turbulent flow of water nanofluids copper oxide in rectangular microchannel with semi attached rib. Adv Mech Eng. 2016;8:1–25.
27. Heydari M, Toghraie D, Akbari OA. The effect of semi-attached and offset mid-truncated ribs and Water/TiO2 nanofluid on flow and heat transfer properties in a triangular microchannel. Therm Sci Eng Prog. 2017;2:140–50.
28. Arani AAA, Akbari OA, Safaei MR, Marzban A, Alrashed AAAA, Ahmadi GR, Nguyen TK. Heat transfer improvement of water/single-wall carbon nanotubes (SWCNT) nanofluid in a novel design of a truncated double layered microchannel heat sink. Int J Heat Mass Transf. 2017;113:780–95.
29. Sarlak R, Yousefzadeh Sh, Akbari OA, Toghraie D, Sarlak S, Assadi F. The investigation of simultaneous heat transfer of water/Al2O3 nanofluid in a close enclosure by applying homogeneous magnetic field. Int J Mech Sci. 2017;133:674–88.
30. Rezaei O, Akbari OA, Marzban A, Toghraie D, Pourfattah F, Mashayekhi R. The numerical investigation of heat transfer and pressure drop of turbulent flow in a triangular microchannel. Physica E. 2017;93:179–89.
31. Akbari OA, Karimipour A, Toghraie D, Safaei MR, Alipour-Goodarzi MH, Dahari M. Investigation of rib's height effect on heat transfer and flow parameters of laminar water- Al_2O_3 nanofluid in a two dimensional rib-microchannel. Appl Math Comput. 2016;290:135–53.
32. Shamsi MR, Akbari OA, Marzban A, Toghraie D, Mashayekhi R. Increasing heat transfer of non-Newtonian nanofluid in rectangular microchannel with triangular ribs. Physica E. 2017;93:167–78.
33. Wei X, Joshi Y, Patterson MK. Experimental and numerical study of a stacked microchannel heat sink for liquid cooling of microelectronic devices. J Heat Transf. 2007;129(10):1432–44.
34. Alrashed AA, Akbari OA, Heydari A, Toghraie D, Zarringhalam M, Ahmadi Sheikh Shabani GHR, Seifi AR, Goodarzi M. The numerical modeling of water/FMWCNT nanofluid flow and heat transfer in a backward-facing contracting channel. Phys B Condens Matter. 2018;537:176–83.
35. Akbari OA, Toghraie D, Karimipour A, Marzban A, Ahmadi GR. The effect of velocity and dimension of solid nanoparticles on heat transfer in non-Newtonian nanofluid. Physica E. 2017;86:68–75.
36. Rahmati AR, Akbari OA, Marzban Ali, Toghraie D, Karimi R, Pourfattah F. Simultaneous investigations the effects of non-Newtonian nanofluid flow in different volume fractions of solid nanoparticles with slip and no-slip boundary conditions. Therm Sci Eng Prog. 2018;5:263–77.
37. Alipour H, Karimipour A, Safaei MR, Semiromi DT, Akbari OA. Influence of T-semi attached rib on turbulent flow and heat transfer parameters of a silver-Water nanofluid with different volume fractions in a three-dimensional trapezoidal microchannel. Physica E. 2016;88:60–76.
38. Tavakoli MR, Akbari OA, Mohammadian A, Khodabandeh E, Pourfattah F. Numerical study of mixed convection heat transfer inside a vertical microchannel with two-phase approach. J Therm Anal Calorim. 2018. https://doi.org/10.1007/s10973-018-7460-z.
39. Rashidi S, Mahian O, Languri EM. Applications of nanofluids in condensing and evaporating systems. J Therm Anal Calorim. 2018;131(3):2027–39.
40. Akar S, Rashidi S, Esfahani JA. Second law of thermodynamic analysis for nanofluid turbulent flow around a rotating cylinder. J Therm Anal Calorim. 2018;132(2):1189–200.
41. Akbarzadeh M, Rashidi S, Karimi N, Omar N. First and second laws of thermodynamics analysis of nanofluid flow inside a heat exchanger duct with wavy walls and a porous insert. J Therm Anal Calorim. 2018. https://doi.org/10.1007/s10973-018-7044-y.
42. Laein RP, Rashidi S, Esfahani JA. Experimental investigation of nanofluid free convection over the vertical and horizontal flat plates with uniform heat flux by PIV. Adv Powder Technol. 2016;27(2):312–22.
43. Rashidi S, Akbarzadeh M, Karimi N, Masoodi R. Combined effects of nanofluid and transverse twisted-baffles on the flow structures, heat transfer and irreversibilities inside a square duct-A numerical study. Appl Therm Eng. 2018;130:135–48.
44. Rashidi S, Javadi P, Esfahani JA. Second law of thermodynamics analysis for nanofluid turbulent flow inside a solar heater with the ribbed absorber plate. J Therm Anal Calorim. 2018. https://doi.org/10.1007/s10973-018-7164-4.
45. Rashidi S, Eskandarian M, Mahian O, Poncet S. Combination of nanofluid and inserts for heat transfer enhancement. J Therm Anal Calorim. 2018. https://doi.org/10.1007/s10973-018-7070-9.
46. Rashidi S, Bovand M, Esfahani JA, Ahmadi G. Discrete particle model for convective AL2O3–water nanofluid around a triangular obstacle. Appl Therm Eng. 2016;100:39–54.
47. Shirejini SZ, Rashidi S, Esfahan JA. Recovery of drop in heat transfer rate for a rotating system by nanofluids. J Mol Liq. 2016;220:961–9.
48. Maskaniyan M, Rashidi S, Esfahani JA. A two-way couple of Eulerian-Lagrangian model for particle transport with different sizes in an obstructed channel. Powder Technol. 2017;312:260–9.
49. Bovand M, Rashidi S, Ahmadi G, Esfahan JA. Effects of trap and reflect particle boundary conditions on particle transport and convective heat transfer for duct flow-A two-way coupling of Eulerian-Lagrangian Model. Appl Therm Eng. 2016;108:368–77.